Field-induced exciton dissociation in PTB7-based organic solar cells

Marina Gerhard,[1,*] Andreas P. Arndt,[2] Mühenad Bilal,[1] Uli Lemmer,[2,3] Martin Koch,[1] and Ian A. Howard[3,†]

[1]*Faculty of Physics and Material Sciences Center, Philipps-Universität Marburg, D-35032 Marburg, Germany*
[2]*Light Technology Institute, Karlsruhe Institute of Technology, D-76131 Karlsruhe, Germany*
[3]*Institute of Microstructure Technology, Karlsruhe Institute of Technology, D-76344 Eggenstein-Leopoldshafen, Germany*

The physics of charge separation in organic semiconductors is a topic of ongoing research of relevance to material and device engineering. Herein, we present experimental observations of the field and temperature dependence of charge separation from singlet excitons in PTB7 and $PC_{71}BM$, and from charge-transfer states created across interfaces in $PTB7/PC_{71}BM$ bulk heterojunction solar cells. We obtain this experimental data by time-resolving the near infrared emission of the states from 10 K to room temperature and electric fields from 0 to 2.5 MV cm^{-1}. Examining how the luminescence is quenched by field and temperature gives direct insight into the underlying physics. We observe that singlet excitons can be split by high fields, and that disorder broadens the high threshold fields needed to split the excitons. Charge-transfer (CT) states, on the other hand, can be separated by both field and temperature. Also, the data imply a strong reduction of the activation barrier for charge splitting from the CT state relative to the exciton state. The observations provided herein of the field-dependent separation of CT states as a function of temperature offer a rich data set against which theoretical models of charge separation can be rigorously tested; it should be useful for developing the more advanced theoretical models of charge separation.

I. INTRODUCTION

Over the last years, remarkable progress has been made in the field of organic photovoltaics (OPV), although the primary optical excitations in organic semiconductors are excitons, which are electron-hole pairs bound by their mutual Coulomb force that cannot be dissociated by means of thermal energy. In fact, poor screening of charges in a dielectric environment with ϵ_r on the order of 3–4 was the major drawback of first-generation organic solar cells [1,2]. These devices typically consisted of a thin polymer layer sandwiched between two electrodes of different work functions and charge generation was only efficient in the immediate proximity of the electrodes. Later, the introduction of the bulk-heterojunction [3] triggered the development of new material systems with significantly higher performances compared to those of mono- or bilayer devices. Bulk heterojunction devices comprise an interpenetrating network of a donor and an acceptor component, in which excitons can be efficiently quenched at the donor-acceptor interfaces by first creating a charge transfer (CT) state that can then further separate. The ongoing progress in the field recently yielded photoconversion efficiencies beyond 10% [4] for single junction solar cells. For such efficient polymer-fullerene systems, field-independent photocurrent generation has been demonstrated [5–7] suggesting that charge transfer (CT) and subsequent dissociation of the CT state can occur efficiently even at low fields. These striking experimental results pose the question, which mechanisms actually drive efficient exciton dissociation at the interface? A more sophisticated understanding is essential for the rational design of novel material systems, in particular for the better design of nonullerene electron acceptors for solar cells, where incomplete CT dissociation is a relevant issue [8,9].

The approaches to understand charge separation are manifold [10,11]. Many experimental studies have focused on the question of whether CT dissociation occurs via electronically or vibronically excited states, or whether CT dissociation occurs just as efficiently through relaxed interfacial states. Transient absorption studies on different polymer/fullerene systems have demonstrated ultrafast charge generation on a subpicosecond time scale [12–14] and more efficient charge separation after excitation of higher and more delocalized electronic states in the polymer [15], thus supporting the hypothesis of a hot mechanism. The role of charge delocalization and vibronic excess energy has also been investigated by means of quantum dynamical simulations [16,17] offering that delocalized and vibronically excited states could account for efficient exciton dissociation. On the other hand, Vandewal *et al.* have recently demonstrated for an efficient OPV device that the internal quantum efficiency did not depend on the amount of vibronic excess energy, as the internal quantum efficiency was near unity even for the resonant excitation of the relaxed CT state [18]. This view is also supported by time-resolved terahertz spectroscopy, which yielded similar exciton dynamics for excitation above and below the optical band gap [19]. Other authors investigate the possibility of long-range separation, based on the assumption of a rather small tunneling barrier [20] or they emphasize the importance of PCBM crystallites [17,21–23] noting their electron affinity is enhanced compared to single PCBM molecules and they provide more delocalized electronic states, which couple more efficiently to charge separated states.

Alternatively, charge separation through energetically relaxed CT states has been proposed. The existence of both ultrafast separation channels and exciton dissociation via a "cold" mechanism in a bulk heterojunction is possible, the processes are not mutually exclusive. In this work, we study the

---

*marina.gerhard@chemphys.lu.se; Present address: Division of Chemical Physics, Lund University, SE-22100 Lund, Sweden.
†ian.howard@kit.edu

donor/acceptor system PTB7/PC$_{71}$BM, for which significant free charge generation on a subpicosecond time scale is known to occur based on transient absorption experiments [14]. However, a smaller subset of the CT states relax at the interface. These may recombine, radiatively or not, or potentially split to form separated charges. In the present study, we probe the emission of this subset. We find evidence that even these "relaxed" CT states separate efficiently with the help of thermal energy at room temperature [24], suggesting that the high performance of this system is not limited by the presence of "deep" trap states at the interface, in which the electron and hole are strongly bound by their Coulomb attraction. By probing this CT emission, we obtain direct insights into the field- and temperature-dependent charge separation via the energetically relaxed route. Dissociation via relaxed CT states implies that the charges must overcome their mutual Coulomb interaction in a diffusive manner. The underlying driving forces of such a process are subject of ongoing theoretical work and Monte Carlo simulations. It has been proposed that a dipolar layer between donor and acceptor moieties and delocalization could facilitate exciton dissociation [25]. Moreover, the important role of entropy in driving charge separation [26,27] and the influence of the dimensionality [28] have been discussed.

We note that an often considered approach to model exciton quenching is the Onsager-Braun model [29,30]. This model has been successfully fitted to field-dependent luminescence quenching data [31–33], giving reasonable values for the binding energies of the involved excitons. However, an important fitting parameter in this model is the product of carrier lifetime and mobility $\mu\tau$ and it has recently been pointed out [34] that the values for $\mu\tau$ obtained by the Onsager-Braun model are generally too large to account for realistic physical quantities. Additionally, the Onsager-Braun model does not include interfacial dipoles, delocalization or effects of disorder in polymeric donor-acceptor heterojunctions.

It is commonly accepted that organic solids, in particular polymeric semiconductors, incorporate disorder with site energies typically spreading over a range of 100 meV [35]. This is of particular relevance for charge and exciton transport and implies that charges escaping from their mutual Coulomb potential do not face a homogeneous medium. Rather, they can be considered to perform hops between sites of different energies within their Coulomb capture radius. These hops can be either exothermic or require a certain activation energy. Therefore the corresponding hopping rates can vary over orders of magnitude. These dispersive transport characteristics have been recognized already two decades ago and were implemented in Monte Carlo simulations [35–38]. Beside the assumption of a disordered lattice, further ideas, such as a higher separation of charges at the interface [39], higher mobility in ordered domains [40], hole delocalization along the polymer chain [41] or the occurrence of hot CT states [42] have been evaluated. However, despite their success in reproducing the experimentally observed recombination kinetics or the field-dependent photocurrent yield, it is not trivial to translate these findings into an analytic kinetic model. In fact, often the parameters required for such modeling are unphysical. In a recent study, Jones *et al.* [43] attempt to consider the manifold of sites involved in hopping dissociation

as a quasifree intermediate state, which is in equilibrium with the CT state. Their kinetic model gives good fits with Monte Carlo data but only when transport rates significantly below the expected values are assumed. These results emphasize the general challenge of including dispersive hopping transport in kinetic modeling.

In the present work, we provide a set of experimental data on the field and temperature dependence of charge carrier separation against which theoretical models and Monte Carlo simulations can be tested. In order to estimate the energy barriers opposed to exciton separation, we apply a one-dimensional analytical model to approximate the field- and temperature-dependent luminescence yield [44]. Although this neglects entropic contributions likely important to more accurately describe the physics of charge separation in the higher dimensional charge motion in the real bulk heterojunction, this one-dimensional model provides an accessible method of highlighting and discussing aspects of our data set. We hope that more advanced and accurate physical insight will be gained by further development of theoretical models and Monte Carlo simulations that are beyond the scope of this initial analysis. We note that recently, this one-dimensional theoretical framework has been applied by Köhler and coworkers, and given good fits to experimentally determined field-dependent photocurrent yields [34,45]. Within this framework, effects of delocalization, interfacial screening, and disorder can be acceptably approximated by modifications of the electrostatic potential.

In our study, we measure both the field- and temperature-dependent luminescence quenching in the OPV system PTB7/PCBM for singlet excitons in the polymer phase, the fullerene phase, and the interfacial CT states at the polymer/fullerene interface. This luminescence quenching provides a direct mechanism to study the field and temperature dependence of electron-hole separation from both the singlet exciton, and the relaxed charge-transfer state [24,46,47]. Therefore these data are a robust test for theoretical models, as one can test whether both the temperature and the field dependencies of the separation are correctly captured by the theory. Moreover, our results are complementary to studies of the field-dependent photocurrent that probe changes in charge separation through all channels, not only the relaxed CT channel to which our experiments are sensitive.

The paper is structured in the following way. After introducing the experimental methods and the theoretical framework for field-assisted hopping in greater detail, we first investigate the quenching of singlet excitons in PTB7 and PCBM and estimate the relevant binding energies and disorder scales from fits of the model presented by Rubel *et al.* In order to test the consistency between the model and the experimentally observed photoluminescence (PL) decay kinetics, we then reconstruct PL transients from the model parameters and compare their dynamics to the experimental results, for which we find good agreement. Afterwards, we focus on the quenching of the interfacial CT state in a PTB7/PCBM blend. CT quenching is found to be efficient already at low electric fields and moderate temperature, indicating that the barrier to charge separation in the CT state is significantly lower than in the singlet exciton state. Further modifications of the kinetic model in terms of a reduced dissociation path, spatially

separated electron and hole sites, and random orientation of the CT states in the electric field are discussed. These discussions serve to highlight interesting aspects of the data set, whose physical origin warrants theoretical scrutiny.

II. EXPERIMENTAL METHODS

The organic solar cells under investigation are bulk heterojunctions formed by PTB7 (thieno-[3,4-b]-thiophene-alt-benzodithiophene) and the fullerene derivative PC$_{71}$BM ([6,6]-phenyl-C$_{71}$-butyric acid methyl ester) as the active layer. For fabrication of the blend film, both components were dissolved in dichlorobenzene solution with a PTB7:PC$_{71}$BM weight ratio of 1:1.5. In addition, 4% of the solvent additive diiodooctane (DIO) were added, which is known to result in a more favorable morphology for charge extraction [48]. The active layer was annealed for 10 min at a temperature of 60 °C. Devices were fabricated in an inverse architecture with indium tin oxide (ITO) as electron-selective and aluminum as hole selective contact. From characterization in a solar simulator we determined a photoconversion efficiency of 7.5% (see Fig. 1). The layer thickness was measured with a profilometer, yielding 72.5 ± 2.5 nm. Another device structure was made from a neat PTB7 film, this had a thickness of 120 ± 2.5 nm.

The devices were mounted in a helium flow cryostat, allowing us to apply electric fields and investigate the temperature range between 10 and 290 K. A Keithley 238 sourcemeter was used to apply a constant bias and to acquire current-voltage curves. For field-dependent studies, the devices were biased in reverse direction. In order to avoid field-induced sample degradation causing a nonreversible decrease of the PL intensity, the exposure times to electric field were kept brief. For each quenching curve, a sequence of PL images was acquired and the bias was turned on and off in an alternating manner for defined time intervals. From this, a control value for the PL intensity could be specified for each bias step by mediating between the preceding and subsequent control measurement. The full set of field- and temperature-dependent data is available in the Supplemental Material [49]. To substantiate that the observed PL quenching is in fact induced by an electric field and not the result of carrier-induced

quenching from the photocurrent or injected current, we also performed quenching measurements in forward direction. According to the asymmetric shape of the current-voltage curves, the currents under forward bias are much higher for a given bias. Adjusting the forward current to an extent, for which remarkable quenching was observed in reverse direction, however, did not lead to any observable quenching effects [49]. Furthermore, we varied the excitation intensity over one order of magnitude for both the neat PTB7 and the blend film without observing significant changes in the quenching curves [49]. From this, we conclude that the quenching is in fact due to the applied electric field and not resulting from the current.

For time-resolved photoluminescence (TRPL) measurements, we used a streak camera, which was operated in the synchroscan mode, in combination with an 80-MHz wavelength-tunable titanium sapphire oscillator, yielding pulses of approximately 100 fs duration in the operating range of wavelengths between 700 and 1000 nm. Optionally, the second harmonic could be generated using a lithium triborate crystal. In order to excite the singlet excitons in the neat PTB7 film, an excitation wavelength of 450 nm was chosen. The fullerene phases of the blend can be selectively excited with a wavelength of 400 nm [24,48]. The excitation beam was oriented perpendicular to the sample and the luminescence was collected with a collimating and a focusing lens at an oblique angle. The field-induced quenching of PCBM excitons was investigated only in the PTB7/PCBM blend, as a pure fullerene device could not be made of sufficient quality to withstand the high fields we employ in our study. For selective excitation of the polymer in the PTB7/PCBM mix phase in the blend film, the laser wavelength was set to 705 nm. This excitation also leads to the formation of emissive interfacial CT states [24]. The time resolution of the experiment is limited by the streak system, and is between 15 and 25 ps depending on the time window and the aperture size for PL detection.

III. KINETIC MODEL

From the experimental data, field-dependent quenching curves for the emission of a given species can be obtained via

$$Q(F,T) = 1 - \frac{I(F,T)}{I(0 \text{ V m}^{-1},T)}, \qquad (1)$$

where $I(F,T)$ denotes the PL intensity of the species for a given applied field and temperature and $I(0 \text{ V m}^{-1}, 0 \text{ K})$ is the PL intensity without external field and at the lowest temperature measurable. Increased quenching of the emission of a given species is directly related to an increased chance of its separation, either due to the excess thermal energy or the potential provided by the electric field. Therefore the key results of this manuscript are the experimental PL quenching curves showing how excitons and charge-transfer excitons can be separated in this system as a function of field and temperature.

Our approach is based on the field-dependent dissociation rate introduced by Rubel *et al.* [44]. In their model, they consider charges which can move via hopping transport on a one-dimensional chain. The separation between the sites is
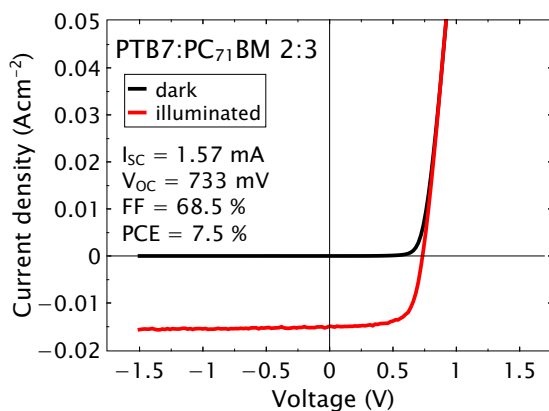

FIG. 1. Current-voltage characteristics of the investigated PTB7/PC$_{71}$BM device measured in a solar simulator and corresponding solar cell parameters.
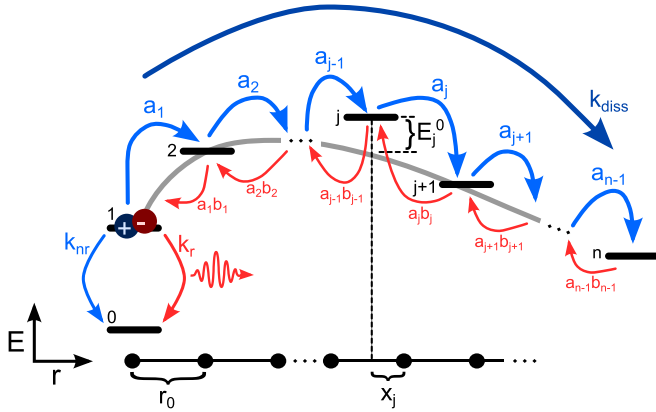
FIG. 2. Kinetic model of a carrier escaping from the Coulomb potential via incoherent hopping between discrete sites with an average spacing r_0 [44]. After optical excitation, site No. 1 is populated either directly in case of singlet excitons, or indirectly via a CT reaction from a singlet precursor state. From the first site, electrons and holes can either recombine or a carrier can hop to an adjacent site. a_j denotes the hopping rate from site j to site $j+1$. The field-induced dissociation rate k_{diss} results from the ensemble of individual hopping rates a_j. The charges are considered to be free when the escaping carrier reaches a site at a critical distance, nr_0. Spatial and energetic disorder are taken into account by x_j and E_j^0 that are random displacements from the spatial lattice and the energy levels. Full details of the model are found in the text.

determined by a lattice parameter r_0 and their energy is given by the Coulomb potential of the opposite charge at the origin, which is altered when an electric field is applied. In such a model system, the spatial and energetic disorder of the sites can be easily implemented by adding a random offset to the position and energy to the original values of the individual sites. Figure 2 shows a schematic representation of the energy levels and transition rates encompassed in their model.

The measured PL intensity $I(F,T)$ is proportional to the probability for radiative recombination

$$\eta(F,T) = \frac{k_r}{k_r + k_{nr} + k_{\mathrm{diss}}(F,T)}, \qquad (2)$$

where k_r and k_{nr} denote the rates for radiative and nonradiative decay, respectively. We note that for calculation of $Q(F,T)$, the absolute radiative rate k_r is not needed. Inserting Eq. (1) into Eq. (2) yields

$$Q(F,T) = 1 - \frac{k_r + k_{nr}}{k_r + k_{nr} + k_{\mathrm{diss}}(F,T)}, \qquad (3)$$

where the sum $k_r + k_{nr} = \tau_{\mathrm{Tot}}^{-1}$ represents the inverse of the exciton lifetime, which can directly be accessed in the time-resolved experiments. We assume that at zero field and 10 K $k_{\mathrm{diss}} = 0$. An analytic form for the field-dependent dissociation rate $k_{\mathrm{diss}}(F,T)$ has been derived by Rubel *et al.* using the model sketched in Fig. 2 [44]:

$$\frac{1}{k_{\mathrm{diss}}(F,T)} = \sum_{j=1}^{n-1} \frac{1}{a_j(F)} \exp\left(\frac{E_j(F) - E_1}{k_B T}\right). \qquad (4)$$

Here, k_B is the Boltzmann constant, T the temperature, and a_j denotes the transition rate from site j to $j+1$ [50]:

$$a_j = \nu_0 \exp\left(-\frac{2(r_{j+1} - r_j)}{\alpha} - \frac{E_{j+1} - E_j + |E_{j+1} - E_j|}{2k_B T}\right). \qquad (5)$$

The first expression in the argument of the exponential function is a tunneling term considering the spatial separation $r_{j+1} - r_j$ between the sites and with α representing the localization length of the carriers. The second term accounts for different site energies such that a thermal activation factor impedes transitions to sites with higher energies. In order to include spatial disorder, the position of each site is determined via $r_j = jr_0 + x_j$, where r_0 is the equidistant spacing of sites in the absence of disorder and x_j is a randomly chosen value from a defined interval $\pm\delta r$. Concordantly with Ref. [44], we calculate the site energies in the Coulomb potential of an oppositely charged carrier at the origin using

$$E_j(F) = E_j^0 - \frac{e^2}{4\pi\epsilon_0\epsilon_r r_j} - eFr_j \qquad (6)$$

with the elementary charge e, vacuum permittivity ϵ_0, and dielectric constant ϵ_r. This definition of the site energies assures that the Coulomb potential is not divergent at the origin. Energetic disorder is implemented with the term E_j^0, which is a random value from a Gaussian distribution centered around zero with standard deviation σ.

The presence of disorder implies that the dissociation probability is individual for each exciton. In order to average sufficiently over the randomly created separation paths, 10^4 runs of the simulation were performed for each temperature. To obtain good fits, we varied the parameters r_0, α, σ, and δr, until a parameter set matching the whole investigated range of temperatures was found. We consider dissociation to be complete when the escaping charge has reached site No. 30. For this distance, the mutual Coulomb potential is ≈ 15 meV, which is within the range of potential fluctuations induced by energetic disorder. In order to describe the high dissociation yield of the CT states, we found it necessary to implement several modifications in the model described above. These modifications will be discussed in Sec. IV.

IV. RESULTS AND DISCUSSION

Figure 3 shows exemplary TRPL data for a temperature of 10 K and a variety of electric fields. The field-dependent quenching characteristics of PTB7 excitons were studied for a neat film with an excitation wavelength of 450 nm. To investigate PCBM excitons, we selectively generate excitons in the fullerene domains of the PTB7/PCBM blend film with an excitation wavelength of 400 nm. The respective spectra and transients are shown in the upper and middle row of Fig. 3. In both cases, the maxima of the spectra exhibit only a slight redshift with increasing field ($\leqslant 10$ meV over the investigated range), indicating that Stark effect plays only a minor role and can be neglected. Importantly, for the PTB7 excitons, the PCBM excitons, and the interfacial CT excitons, the PL lifetime becomes shorter with increasing electric fields. Therefore all of the species show field-assisted dissociation
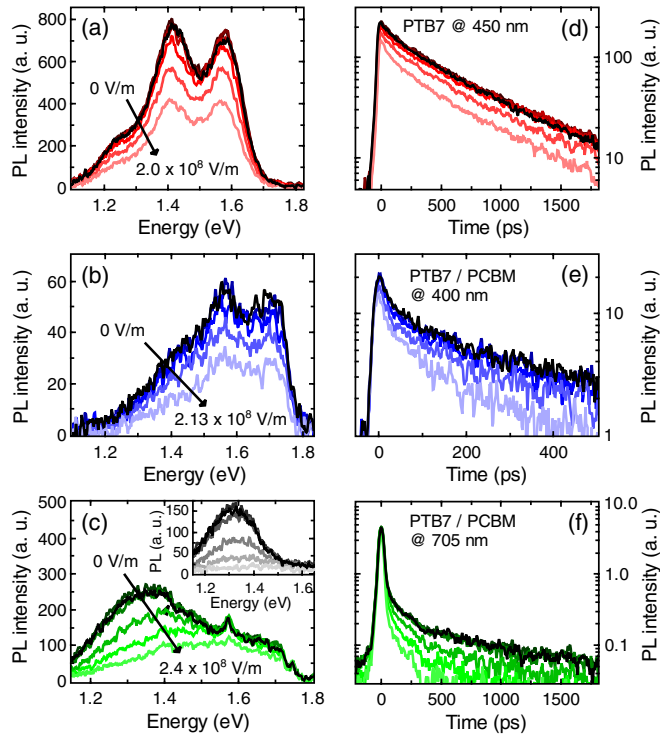
FIG. 3. Recorded PL spectra (a)–(c) and transients (d)–(f) for different electric fields at a sample temperature of 10 K. The black curves represent control measurements without applied bias. The data in (a) and (d) were obtained from a neat PTB7 film under 450 nm excitation. The data in (b) and (e) are attributed to PCBM excitons, which can be selectively probed in the PTB7/PCBM blend film with an excitation wavelength of 400 nm. (c) and (f) show PL spectra and transients of the PTB7/PCBM blend for an excitation wavelength of 705 nm. In this case, the recorded PL signal is a superposition of singlet and CT emission. The inset in (c) shows the field-dependent spectra of only the CT signature, obtained by integrating the recorded TRPL data over the time interval between 100 and 2000 ps after optical excitation.

indicating that they can all be separated with an electric field. In the following, we will look at the field and temperature dependence of the separation for each of the species in turn. We also note that in the recorded data and the quenching parameters we derived from it, we found no influence of any "hot" precursor states of the excitonic population, neither in the early PL spectra, nor in terms of a "static" PL quenching with applied field [49].

Figures 3(c) and 3(f) show the field-dependent PL spectra and transients for the blend film after 705 nm excitation. In this case, the PL comes from both singlet excitons and CT states [24]. The singlet excitons are much shorter lived though, and the emission after 100 ps comes exclusively from the CT states. The emission of these two states with different lifetime ranges is apparent in the PL decay dynamics. The short-lived component results from singlet states and decays very quickly, due to charge transfer at internal interfaces of the bulk heterojunction. The longer-lived contribution is attributed to CT emission. In the integrated PL spectra in Fig. 3(c), the peak blue shifts with the application of field, we will see that this is due to the fact that CT states are

separated more easily with field than the singlet excitons. This leads to a more significant quenching of the CT emission than the PTB7 singlet exciton emission as fields are applied, and therefore the shift of the net PL peak towards the bluer emission peak of the singlet excitons. To illustrate only the field dependence of the PL of the CT states, we integrate the emission in the time range between 100 and 2000 ps after optical excitation, thus excluding the PL contribution of the singlet excitons. These data are presented in the inset of Fig. 3(c). These data demonstrate that the magnitude of the CT emission is drastically reduced by the presence of an electric field, and also that the peak of the CT emission itself does not shift significantly with applied field. From fitting Gaussians to these CT peaks, we derive a net blueshift of the CT signature on the order of 20 meV, when the external field is increased from zero to an extent of 2.5×10^8 V m^{-1}. Also, its linewidth is broadened by about 36%. This slight blue-shifting and broadening is consistent with the average electron hole distance in the CT state perhaps increasing slightly, and the variety of distances slightly increasing with field. However, the main observation is the very clear dependence of the CT emission intensity and lifetime on electric field that we investigate further in the next sections.

From the experimental data, field-dependent quenching curves are obtained using Eq. (1), which relates the PL intensity at zero field to the PL intensity for a certain bias, normalized to the zero-field emission for that given temperature. The PL intensity of the PTB7 singlet emission was calculated from integrated emission of the neat PTB7 film, that is the integral over the data presented in Figs. 3(a) and 3(b) (and similar for different temperatures). In order to obtain the PL intensity of the CT states, the emission of the blend after excitation at 705 nm was used, and the time interval after 100 ps was approximated with a biexponential fit function, which we found to be a good approximation for the complex CT dynamics. The fitting allows all of the CT emission to be counted, without counting unwanted emission from short-lived singlet exciton states. The CT intensity was estimated from the integral over this model function (see Ref. [49]). The emission of the PC$_{71}$BM singlet excitons was determined by integrating the emission of the blend after 400-nm excitation, i.e., the data shown in Figs. 3(d) and 3(e) (and similar for other temperatures).

Quenching curves for the different excited species at a temperature of 10 K are presented in Fig. 4(a). Comparing the curves, one notes that the CT emission starts to be quenched at fields considerably smaller than those required to quench the emission from singlet states on the PTB7 or the PCBM. This makes sense in that it indicates that the CT states are more weakly bound than the singlet exciton states. The quenching curves do not have a sudden onset. To consider what this implies about the underlying microscopic mechanisms leading to exciton dissociation, we compare in Fig. 4(b) curves of the PTB7 exciton quenching with the Onsager-Braun model. In the Onsager-Braun model, the field- and temperature-dependent dissociation rate k_{diss} is given by [29,30]

$$k_{\text{diss}}(F,T) = \frac{3e\mu}{4\pi r_0^3 \epsilon_0 \epsilon_r} \exp\left(-\frac{E_b}{k_B T}\right) \frac{J_1(2\sqrt{-2b})}{\sqrt{-2b}}, \quad (7)$$
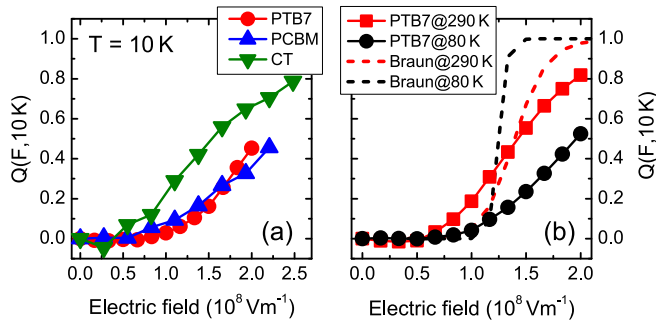
FIG. 4. Field-induced PL quenching of the neat PTB7 film emission and for the PTB7/PCBM device after selective excitation of the PCBM domains and the intermixed phases, respectively. The sample temperature for the quenching curves presented in (a) was 10 K. In (b), quenching curves of the PTB7 emission are presented for 290 and 80 K. The dotted curves show the modeled quenching behavior, as predicted by the Onsager-Braun model [with parameters $\epsilon_0 = 3$, $\mu\tau_r = 10^{-17}$ V^2 m^{-1}, and $r_0 = 1.04$ nm according to Eqs. (6) and (8)].

with carrier mobility μ and initial separation of the charges r_0. The parameter $E_b = e^2/4\pi\epsilon_0\epsilon_r r_0$ denotes the binding energy of the charge pair and J_1 is the first-order Bessel function with $b = e^3 F/8\pi\epsilon_0\epsilon_r(k_B T)^2$. When radiative recombination with time constant τ_r is the only decay channel beside field-induced dissociation, Eq. (2) for the field-dependent recombination probability can be rewritten as

$$\eta(F,T) = \frac{1}{1 + \tau_r k_{\text{diss}}(F,T)}. \tag{8}$$

Using Eq. (1), (6), and (8), the quenching yield, as predicted by the Onsager-Braun model, was calculated using estimations for the parameters of $\epsilon_0 = 3$, $\mu\tau_r = 10^{-17}$ V^2 m^{-1} and $r_0 = 1.04$ nm. The corresponding quenching curves for temperatures of 290 and 80 K are presented in panel (b) of Fig. 4. We note that even at room temperature the slope of the experimental quenching curve is much shallower than in the Onsager-Braun model and this discrepancy increases with decreasing temperature. Similar problems to match the experimental data were obtained when the disorder parameters in the model presented in Ref. [44] were set to zero. In the limit of low temperatures, both the Onsager-Braun and the Rubel kinetic models predict an almost steplike increase of the quenching yield at a certain threshold voltage, which is related to the binding energy. The fact that we observe a gradual increase in quenching with field, even at low temperatures suggests that there is not a single binding energy, but rather that the binding energy of a given state is strongly affected by its environment. We examine this hypothesis in the following, where we consider disorder effects by applying the theoretical framework suggested Rubel *et al.* [44].

Theoretical quenching curves based on the field- and temperature-dependent dissociation rate according to Eq. (3) are presented in Fig. 5, together with experimentally obtained quenching curves for the singlet excitons. The corresponding parameter sets are summarized in Table I. The parameter ϵ_r was set to 3.0 for PTB7 and 3.9 for PCBM, respectively, according to the values typically reported in the literature [33,44,51–53].
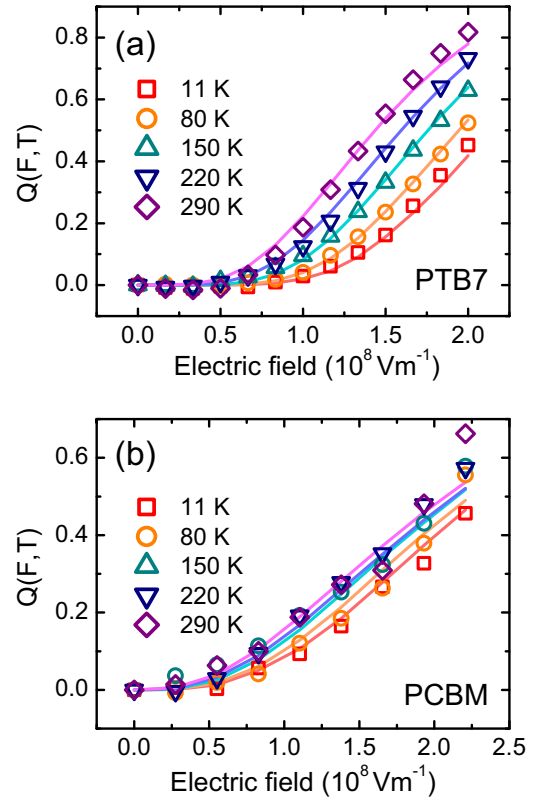

FIG. 5. Temperature-dependent luminescence-quenching curves for PTB7 and PCBM singlet excitons. The PL of the neat PTB7 film was recorded after 450-nm excitation. PCBM excitons were probed in the PTB7/PCBM blend, after excitation at 400 nm. The symbols represent experimental data. Solid lines are theoretical quenching curves, as predicted by the model suggested by Rubel *et al.* [44]. The parameter sets we used for fitting the data are summarized in Table I.

In both cases, we used a fixed value of $\nu_0 = 10^{13}$ s^{-1} for the attempt-to-escape frequency, again in accordance with previous estimates for this parameter [34,44]. A general problem for the accuracy of our approach arises from the

TABLE I. Model parameters corresponding to the theoretical quenching curves in 5. The parameters α, r_0, δr, and σ were varied to match the experimental data, whereas the other parameters were kept fixed. In case of PCBM, we used different values for the parameter τ_{Tot}, according to the diffusion-related faster decay with increasing temperature: 110 ps at 10 K, 98 ps at 80 K, 94 ps at 150 K, 70 ps at 220 K, and 65 ps at 290 K. The energy E_1 represents the energy level of the first site in the disorder- and field-free Coulomb potential and thus can be interpreted as the average exciton binding energy.

Parameter description	Parameter	PTB7	PCBM
Dielectric constant	ϵ_r	3	3.9
Attempt-to-escape frequency	ν_0 (s^{-1})	10^{13}	10^{13}
Singlet lifetime without ext. field	τ_{Tot} (ps)	500	65–110
Site separation	r_0 (nm)	1.06	0.94
Localization length	α (nm)	0.46	0.43
Spatial disorder parameter	δr (nm)	0.08	0.20
Energetic disorder parameter	σ (meV)	49	80
Energy of first site	E_1 (meV)	452	393

discrepancy between the applied electric field and the actual field faced by the excitons. Lacking a better methodology, we make the assumption that the field is uniform across the device. The layer thicknesses were determined with a precision of 5 nm, which translates into a maximum inaccuracy of $\pm 8.6 \times 10^6$ V m^{-1} for the highest applied field in the blend device. In order to match the experimental data, the parameters $r_0, \alpha, \delta r$ and σ were varied and the same set of parameters was used to fit the data of the whole temperature range between 10 and 290 K.

In Fig. 5, we show that the model can reproduce the measured curves well, confirming that spatial and energetic disorder have a strong influence on the temperature-dependence of the quenching curves. The most important effect is the broadening of the quenching threshold, resulting from the superposition of many random dissociation paths in a disordered density of states, each yielding an individual threshold for field-induced quenching. The disorder parameters for the PCBM excitons in the blend film are higher than those obtained for the neat PTB7 device, which is consistent with the morphology in the blend being less uniform than in a single-component film. The disorder parameters we extract agree well with those found using other methods in recent literature reports [53–55]. In case of PCBM, we insert the measured exciton lifetimes of the PCBM emission in the blend into Eq. (2), thus, the possibility for PCBM excitons to get quenched at interfaces to PTB7 is intrinsically included in our modeling. The values of τ_{Tot} for the PCBM emission at different temperatures are listed in the caption of Table I. The quenching curves of the PCBM excitons show weaker temperature dependence than those obtained for PTB7 excitons. This is due to the additional option for PCBM excitons to be quenched at interfaces in the blend with PTB7, reducing the influence of the field-induced (and temperature-dependent) quenching rate. The amount of energy a carrier needs to escape from its mutual Coulomb potential can be interpreted as the binding energy of the electron-hole-pair. In a disordered material system, a manifold of binding energies determines the actual quenching characteristics. However, an average binding energy can be derived by calculating the energy level $E_1 = e^2/4\pi\epsilon_0\epsilon_r r_0$, which represents the energy of the first site in the Coulomb potential in the absence of disorder and an electric field. For the neat PTB7 film, the parameter set in Table I yields a value of 452 meV. This is in the range of binding energies, which is typically expected for singlet excitons in polymers. For example, the binding energy of excitons in PPV-type polymers was estimated to 300–400 meV by means of the Onsager-Braun theory [33,37] and Monte Carlo simulations [36]. For P3HT, an energy barrier of 420 meV has been determined for polaron pair generation [32]. For PTB7, it has been suggested that the exciton binding energy could be significantly lowered due to the high built-in polarization of the alternating electron-rich and electron-poor monomer units [14], however, our results suggest that the singlet excitons on PTB7 are still strongly bound.

This simple model fits the field dependence for given temperatures well, but we now check how well it reproduces the experimentally observed decay dynamics. In order to compare these data to the model predictions, transients had to be constructed from the simulations. We constructed the
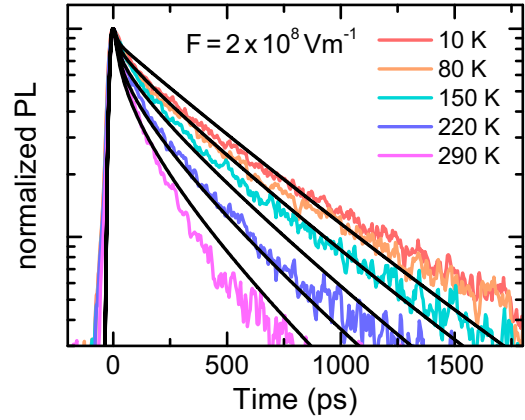

FIG. 6. Comparison of experimental transients recorded under an external field of 2×10^8 Vm^{-1} and simulated transients according to Eq. (9).

model transients as superpositions of the PL decay for 10^4 repetitions of individual quenching paths for each field and temperature. Furthermore, the instrument's response has to be taken into account by convolving the theoretical transient with the instrument response function:

$$I(t) = \int_{-\infty}^{\infty} \exp\left(-\frac{(t'-t)^2}{2w^2}\right)$$
$$\times \sum_{j=1}^{M} \exp(-(k_{\text{Tot},j} + k_{\text{diss},j})t')\Theta(t')dt'. \quad (9)$$

Here, w is the rise time of the pulse response function, for which we used a value of 10 ps, according to the experimental rise time of the PL transients. M is the number of simulation runs, over which the transient was averaged, the sum $k_{\text{Tot}} + k_{\text{diss}}$ is the inverse exciton lifetime and $\Theta(t)$ is the Heaviside function, which accounts for a rise of the PL signal at $t = 0$.

Using the same parameter set used to fit the PTB7 singlet excitons in the neat film shown in Table I, we find reasonable agreement between the experimentally observed PL dynamics and the predictions of the model as shown in Fig. 6. The satisfying match between experimental and theoretical data both in terms of the energetic dependence of quenching, and its dynamics in time give us confidence that this simple model is indeed describing most of the physics relevant to carrier dissociation in this system and encourages us to use this simple framework to look at our data on CT dissociation in more detail.

We will now turn from the data on the PL quenching of the singlet excitons to the PL quenching for the CT state. One fundamental difference between the singlet and the CT PL characteristics must be considered, although the singlet emission is not quenched by increasing the temperature, the CT emission is. In previous work on PTB7/PCBM, we found a surprisingly small activation barrier for thermal CT quenching on the order of 30 meV [24]. For the singlet states on the other hand, no noticeable temperature dependence of the PL intensity was observed, except for a slight diffusion-related decrease of the decay-times in case of the PCBM singlet excitons. Thus we must consider how CT states are separated
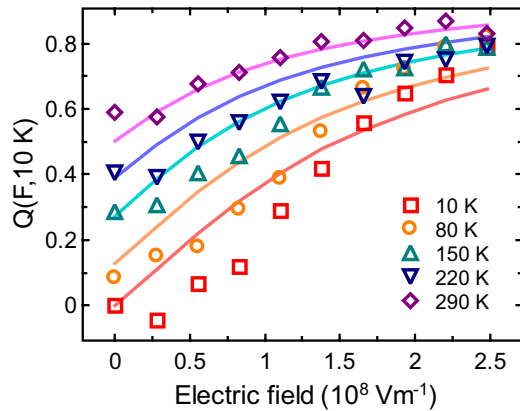
FIG. 7. Measured CT intensity quenching showing the field and temperature dependence of CT separation at the PTB7/fullerene interface (symbols). Simulation results for separation of carriers by hopping between sites in a disordered but flat potential (solid curves) reproduce the data well, suggesting that the Coulomb potential is strongly screened by the interface.

FIG. 8. Schematic of the energetics for (a) separation of singlet states and (b) separation of CT states. E_1 denotes the effective activation barrier, the gray-shaded area corresponds to the expected fluctuations of the energy levels described by the disorder parameter sigma, and x_0 is the initial separation of the charges populating a CT state. In case of the CT states, the range of spatial disorder is indicated by the darker gray areas and the parameter δr.

by both field and temperature at the same time, not just how the field dependence changes as a function of temperature. To do this, the measured and simulated PL quenching yields are normalized to the maximum CT intensity, which is measured with no applied field and at a sample temperature of 10 K. Thus the quenching curves are calculated as $Q(F,T) = 1 - I(F,T)/I(0,10\,\mathrm{K})$. These experimental values are presented in Fig. 7, which provides a rich data set revealing how CT states are separated by both temperature and field. We consider this dataset to be the primary contribution of this work, as it provides an important test for models and theories of CT separation at organic heterojunctions.

In order to obtain a reasonable fit to this experimental data with the kinetic model, one major modification must be made with respect to the parameters for the singlet-exciton case. That is, the carrier must be assumed to hop in a much flatter potential. In order to qualitatively fit both the temperature and field dependence of the CT state separation, we find it necessary to empirically reduce the Coulomb term in Eq. (5) by a factor of 10. With this modification, the kinetic model can give good agreement with the experimental CT quenching data. The reduction of the Coulomb term leads to a flattening of the potential well close to the interface, such, that thermally and field-induced dissociation can easily occur from the first site. We note that reducing the Coulomb term does not necessarily imply weaker Coulomb interactions between the charges. Beside dielectric screening, other physical phenomena could account for the lower barrier for charge separation. We will further discuss several scenarios in the next section and we anticipate that more advanced modeling will reveal more accurate insight into the fundamental physical processes that underlie this behavior. To graphically illustrate this flattening of the potential, the site energies for singlet and CT states in the absence of an external field are presented schematically in Fig. 8.

When considering a highly reduced potential well, it is also necessary to revisit the criterion for charge dissociation, because the first or second site energy level is already in the
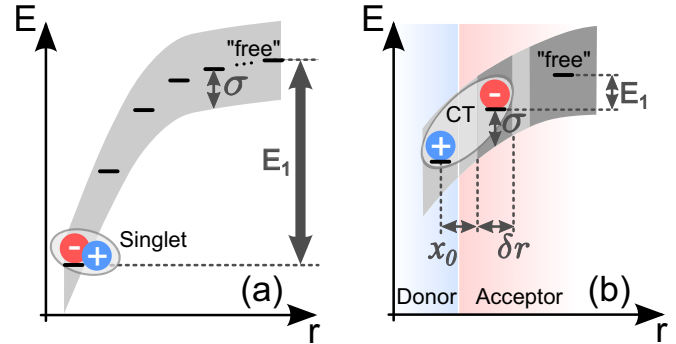
range of thermal or disorder-induced energetic fluctuations. The hopping rates are thus governed by the energetic disorder rather than by the potential well. This implies that dissociation occurs after a much smaller number of sites, because the potential is masked by the disordered environment already after a few separation steps. In fact, in order to reproduce the strong temperature dependence of the CT quenching data, we found the best match for considering the minimum of $n = 2$ sites. For longer dissociation paths, the temperature dependence was found to be underestimated by the model (see Ref. [49]). It should also be considered that the charges populating the CT state have some initial separation. As a consequence, the energy level of the first site does not represent the minimum of the potential well. Both an energetically raised first site and a slower rate for radiative decay resulting from increased spatial separation between electron and hole contribute to the increased separation of CT excitons. In the model, we implement spatial separation between the electron and hole sites by adding a fixed spatial offset x_0 to the position of each site [see Fig. 8(b)]. Furthermore, the spatial disorder parameter δr accounts for an additional randomly created spatial offset. For the first site, we generate random offset values x_1 from the interval $[0, \delta r]$, so the average separation between the electron and hole sites in our model is given by the sum $x_0 + \delta r/2$. We found good agreement between the experimental quenching data and the modeling results for a broader range of values for x_0. However, the best agreement with the PL dynamics was obtained for relatively small values of x_0, whereas a value larger than 0.2 nm lead to underestimated decay times of the modeled PL transients.

As a last point we consider is the possibility of CT states to orient in the electric field. As CT states are constrained to the randomly oriented donor-acceptor interfaces, they will not all be oriented in the direction of the applied electric field. It could even occur that the electric field is antiparallel with respect to the CT orientation, implying that for some CT excitons the applied field even enhances the recombination rate. Experimentally, we observe a surprisingly weak field dependence of the CT quenching yield, which could be a consequence of

TABLE II. Model parameters used to approximate the experimental CT quenching curves presented in Fig. 7. Modifications compared to the model for singlet quenching are described in the text. Similar to the modeling of the singlet quenching, the parameters r_0, α, δr, and σ were varied to match the experimental data, whereas the other parameters were kept constant.

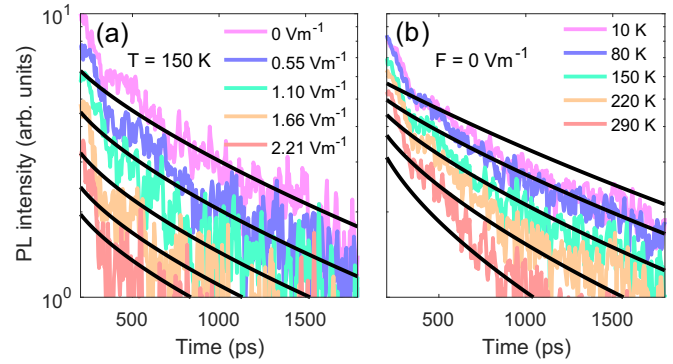| Parameter description	Parameter	Value
Dielectric constant	ϵ_r	3.4
Attempt-to-escape frequency	ν_0 (s^{-1})	10^{13}
CT lifetime without ext. field	τ_{Tot} (ps)	400
Site separation	r_0 (nm)	0.89
Localization length	α (nm)	0.44
Spatial disorder parameter	δr (nm)	0.42
Energetic disorder parameter	σ (meV)	70
Energy of first site	E_1(meV)	35

FIG. 9. Experimental CT transients and reconstructed transients from the modeled dissociation rates, using Eq. (9), both plotted over one order of magnitude. (a) shows the field-dependent decay of the CT PL for a temperature of 150 K. (b) summarizes the temperature-dependent decay characteristics at zero field.

such localization effects. In fact, modeling the CT quenching data with a reasonable set of parameters and using the actually applied electric field yielded stronger field dependencies than experimentally observed (see Ref. [49]). Better matches were obtained either by reducing the experimentally applied field by 25 % or by considering the angular dependence explicitly in the kinetic model. We chose the latter approach and calculated the effective field via $F_{eff}(F) = F \cos(\theta)$, where θ is a random angle from the interval $\pm \pi$, which is individual for each randomly created dissociation path.

The modeled quenching curves for an initial separation of $x_0 = 0.1$ nm between the electron and the hole sites are presented as solid lines in Fig. 7 and the corresponding parameter set is listed in Table II. We note that in case of the CT states, the PL yield is not directly calculated from the parameter τ_{Tot}. Here, τ_{Tot} denotes the hypothetical CT lifetime for the case that electron and hole forming the CT state are not spatially separated. However, the spatial separation between the electron and hole sites leads to a longer actual lifetime $\tau_{\mathrm{Tot},0}$, which is expected to be enhanced by a tunneling term, giving $\tau_{\mathrm{Tot},0} = \tau_{\mathrm{Tot}} \exp(2(x_0 + x_1)/\alpha)$ [44]. Here, x_0 quantifies the spatial separation between electron and hole, x_1 is the randomly created offset of the first site based on the choice of δr, and α is a localization parameter. We estimate the hypothetical value $\tau_{\mathrm{Tot}} = 400$ ps, which is on the order of the PL decay rates of the singlet states. With an average spatial offset of 0.3 nm, this results in $\tau_{\mathrm{Tot},0} \approx 1.6$ ns, which is in good agreement with the experimentally determined CT decay time at low temperature and without applied electrical field. For calculation of the PL yield [Eq. (2)], we used the effective longer CT lifetime $\tau_{\mathrm{Tot},0}$, which was calculated for each individual separation path from τ_{Tot} and the randomly created spatial offset $x_0 + x_1$. A particular difference between the singlet and the CT model parameters is the higher value of the spatial disorder parameter δr used for the CT quenching. In general, both the spatial and the energetic disorder parameter could be increased to match the weak slope of the experimentally observed field-dependent quenching curves. However, in order to reproduce the observed field-and temperature dependent dynamics of the CT emission, we found better agreement for higher values of δr, whereas the

parameter for energetic disorder σ was chosen comparable to the energetic disorder scales of the singlet states. Experimental and modeled transients of the CT emission are presented in Fig. 9. With an appropriate selection of the parameters x_0 and δr, both the temperature and the field-dependent PL dynamics can be reproduced in good agreement with the experimental data. This further suggests that for the PTB7/PCBM system the *relaxed* CT states are quenched by the applied field and that there is a kinetic competition between their separation and recombination. Interestingly, our findings diverge from a recent study on the highly efficient OPV system TQ1/PC$_{71}$BM, where the field has been found to affect in particular the hot and delocalized CT states on a short timescale, whereas the emissive CT state revealed strong trapping character [56]. These different results suggest that the CT binding energy varies strongly among common high-performance OPV systems. For some systems, efficient charge generation may strongly depend on the efficiency of a "hot" separation mechanism, but a "cold" process as observed for PTB7/PC$_{71}$BM can be efficient as well, when the CT states are only weakly bound.

Looking at the parameters, shown in Table II, extracted from this empirical model we note the effective average binding energy of the CT state E_1 is 35 meV. For calculation of E_1, it is important to consider that the electron and hole sites have an average separation of $x_0 + \delta r/2 = 0.3$ nm (see Fig. 8) and thus, the energy of the first site is raised with respect to the potential energy at $r = 0$. We note that the energetic disorder is larger than E_1 with a value of $\sigma = 70$ meV. This again supports the physical picture that at some interfacial sites there is a flat or even energetically favorable pathway for charge separation, whereas at other interfacial sites the CT state is the lowest energy state.

Our experimental and modeling results strongly suggest that charge separation from the donor/acceptor interface is almost barrier-free and both the influence of disorder and the energetic landscape are of extreme relevance to describe the dissociation yield. The data establish that there are remarkable differences between the separation of singlet excitons and CT states. It is beyond the scope of the present work to conclusively establish the physical origin of the low CT stability,

which is likely to contribute to the high photoconversion efficiency reported for the investigated material system [57]. However, these data should be of value to the variety of theoretical approaches that could provide physical insight into the mechanisms that lead to these differences in charge separation [11,17,25–28,40,52,58–62].

In early work on this topic it has been proposed that dielectric screening at the interface and delocalization could help the charges to overcome their mutual Coulomb attraction [25]. Delocalization supplies the charges with some additional kinetic energy and it can be accounted for in terms of an effective mass that is smaller than the free carrier mass [34,63]. Recently, the concept of effective mass has been applied in Monte Carlo simulations and particularly high dissociation yields were established in a two-dimensional model under the assumption that both carriers at the interface are mobile [28]. In this context, it is interesting to mention that the hole mobility in PTB7/PCBM blends was found to rise by three orders of magnitude when the temperature was increased from 77 K to room temperature [64], implying a growing influence of bipolar transport, which could be an explanation for the strong temperature dependence of the CT PL yield. The electrostatics at the interface has also been considered by Poelking and Andrienko [58], who showed that long-range order and molecular mixing at the interface can generate driving forces that support charge separation.

We also highlight that we have not considered in detail the influence of dimensionality, which is likely to play an important role, because an interface of higher dimensionality provides more possible separation pathways for the charges. In their Monte Carlo study, Athanasopoulos *et al.* [28] compared a one-dimensional with a two-dimensional model system and found pronounced differences for the charge extraction yield. An alternative approach to explain the efficient separation of charges at the donor/acceptor interface arises from the consideration of entropy [26,27]. Recently, Hood and Kassal [27] estimated the contribution of entropy to the lowering of the potential energy by summing over all possible spatial configurations of electron and hole with a specific separation distance. In their work, they distinguish between two cases: (i) one of the charges is fixed and (ii) both charges are mobile, which leads to a higher entropic contribution due to different scaling of the entropy term with the distance of the charges.

Finally, we should discuss the role of disorder. On the one hand, disorder will reduce the contribution of entropy to the lowering of the free energy, but likewise, Hood and Kassal [27] have demonstrated that disorder can significantly reduce the barrier to charge separation, because the presence of low-energetic sites provides energetically more favorable separation routes. As an important result, their thermodynamical considerations showed similar contributions of entropy

and energetic disorder for a moderate disorder parameter of $\sigma = 50$ meV, and the Coulomb barrier for charge separation ($\approx$400 meV) virtually vanished for energetic disorder of 100 meV, where the contribution of entropy was very small.

V. CONCLUSION

In this contribution, we have presented a study on the field-induced dissociation of singlet and CT excitons in the PTB7/PC$_{71}$BM OPV system. For both singlet and CT emission, the observed field-dependence does not show sudden onsets, the quenching varies gradually with field at all temperatures. Through our simple modeling, we find that this indicates that inhomogeneous disorder plays a large role in altering the charge separation process between individual interfacial sites. From the analytic modeling approach, we extract the average binding energies of the PTB7 and PC$_{71}$BM singlet excitons as 452 and 393 meV, respectively. The energetic disorder parameters for the PTB7 and PCBM singlet excitons are 49 and 80 meV. For the charge-transfer state at the PTB7/PC$_{71}$BM interface, we find an average binding energy of 35 meV with an energetic disorder of 70 meV. While singlet excitons need significant application of field to separate, CT states can dissociate spontaneously, or with small assistance from thermal energy or the applied field.

Our simple theoretical analysis indicate that in order to fit the data, it is necessary to assume significant flattening of the interfacial potential. Theoretical studies investigating the effects of interfacial dipoles, delocalization, bipolar and multidimensional transport support this hypothesis. In particular, the contributions of entropy and energetic disorder to the free energy could explain the almost barrier-free separation of the charges we observed experimentally. More advanced theoretical models and further experimental data will hopefully reveal the real physical mechanism that manifests itself as field-flattening in our considerations. We believe that this experimental data set revealing the temperature and field dependence of charge separation from singlet exciton states, and from interfacial charge transfer states will prove useful for the testing of more sophisticated theoretical models, and ultimately assist in the deeper physical understanding of the charge separation process.

[1] G. Chamberlain, Sol. Cells **8**, 47 (1983).

[2] W. Rieß, S. Karg, V. Dyakonov, M. Meier, and M. Schwoerer, J. Lumin. **60-61**, 906 (1994).

[3] G. Yu, J. Gao, J. C. Hummelen, F. Wudl, and A. J. Heeger, Science **270**, 1789 (1995).

[4] M. A. Green, K. Emery, Y. Hishikawa, W. Warta, and E. D. Dunlop, Prog. Photovolt: Res. Appl. **23**, 1 (2015).

[5] S. H. Park, A. Roy, S. Beaupré, S. Cho, N. Coates, J. S. Moon, D. Moses, M. Leclerc, K. Lee, and A. J. Heeger, Nat. Photon. **3**, 297 (2009).

[6] G. F. A. Dibb, F. C. Jamieson, A. Maurano, J. Nelson, and J. R. Durrant, J. Phys. Chem. Lett. **4**, 803 (2013).

[7] J. Kniepert, I. Lange, J. Heidbrink, J. Kurpiers, T. J. K. Brenner, L. J. A. Koster, and D. Neher, J. Phys. Chem. C **119**, 8310 (2015).

[8] C. B. Nielsen, S. Holliday, H.-Y. Chen, S. J. Cryer, and I. McCulloch, Acc. Chem. Res. **48**, 2803 (2015).

[9] D. W. Gehrig, I. A. Howard, V. Kamm, H. Mangold, and D. Neher, J. Phys. Chem. C **118**, 20077 (2014).

[10] S. Few, J. M. Frost, and J. Nelson, Phys. Chem. Chem. Phys. **17**, 2311 (2015).

[11] H. Bässler and A. Köhler, Phys. Chem. Chem. Phys. **17**, 28451 (2015).

[12] I. A. Howard, R. Mauer, M. Meister, and F. Laquai, J. Am. Chem. Soc. **132**, 14866 (2010).

[13] M. Tong, N. E. Coates, D. Moses, A. J. Heeger, S. Beaupré, and M. Leclerc, Phys. Rev. B **81**, 125210 (2010).

[14] J. M. Szarko, B. S. Rolczynski, S. J. Lou, T. Xu, J. Strzalka, T. J. Marks, L. Yu, and L. X. Chen, Adv. Funct. Mater. **24**, 10 (2014).

[15] G. Grancini, M. Maiuri, D. Fazzi, A. Petrozza, H.-J. Egelhaaf, D. Brida, G. Cerullo, and G. Lanzani, Nat. Mater. **12**, 29 (2013).

[16] H. Tamura and I. Burghardt, J. Am. Chem. Soc. **135**, 16364 (2013).

[17] M. Huix-Rotllant, H. Tamura, and I. Burghardt, J. Phys. Chem. Lett. **6**, 1702 (2015).

[18] K. Vandewal, S. Albrecht, E. T. Hoke, K. R. Graham, J. Widmer, J. D. Douglas, M. Schubert, W. R. Mateker, J. T. Bloking, G. F. Burkhard, A. Sellinger, J. M. J. Fréchet, A. Amassian, M. K. Riede, M. D. McGehee, D. Neher, and A. Salleo, Nat. Mater. **13**, 63 (2014).

[19] P. D. Cunningham and L. M. Hayden, J. Phys. Chem. C **112**, 7928 (2008).

[20] D. Caruso and A. Troisi, Proc. Natl. Acad. Sci. USA **109**, 13498 (2012).

[21] F. C. Jamieson, E. B. Domingo, T. McCarthy-Ward, M. Heeney, N. Stingelin, and J. R. Durrant, Chem. Sci. **3**, 485 (2012).

[22] B. Bernardo, D. Cheyns, B. Verreet, R. D. Schaller, B. P. Rand, and N. C. Giebink, Nat. Commun. **5**, 3245 (2014).

[23] B. M. Savoie, A. Rao, A. a. Bakulin, S. Gelinas, B. Movaghar, R. H. Friend, T. J. Marks, and M. A. Ratner, J. Am. Chem. Soc. **136**, 2876 (2014).

[24] M. Gerhard, A. P. Arndt, I. A. Howard, A. Rahimi-Iman, U. Lemmer, and M. Koch, J. Phys. Chem. C **119**, 28309 (2015).

[25] V. I. Arkhipov, P. Heremans, and H. Bässler, Appl. Phys. Lett. **82**, 4605 (2003).

[26] T. M. Clarke and J. R. Durrant, Chem. Rev. **110**, 6736 (2010).

[27] S. N. Hood and I. Kassal, J. Phys. Chem. Lett. **7**, 4495 (2016).

[28] S. Athanasopoulos, S. Tscheuschner, H. Bässler, and A. Köhler, arXiv:1611.00427.

[29] L. Onsager, J. Chem. Phys. **2**, 599 (1934).

[30] C. L. Braun, J. Chem. Phys. **80**, 4157 (1984).

[31] M. Hallermann, S. Haneder, and E. Da Como, Appl. Phys. Lett. **93**, 053307 (2008).

[32] C. Deibel, D. Mack, J. Gorenflot, A. Schöll, S. Krause, F. Reinert, D. Rauh, and V. Dyakonov, Phys. Rev. B **81**, 085202 (2010).

[33] J. Kern, S. Schwab, C. Deibel, and V. Dyakonov, Phys. Status Solidi RRL **5**, 364 (2011).

[34] C. Schwarz, S. Tscheuschner, J. Frisch, S. Winkler, N. Koch, H. Bässler, and A. Köhler, Phys. Rev. B **87**, 155205 (2013).

[35] H. Bässler, Phys. Status Solidi B **175**, 15 (1993).

[36] M. Scheidler, U. Lemmer, R. Kersting, S. Karg, W. Riess, B. Cleve, R. F. Mahrt, H. Kurz, H. Bässler, E. O. Göbel, and P. Thomas, Phys. Rev. B **54**, 5536 (1996).

[37] S. Barth and H. Bässler, Phys. Rev. Lett. **79**, 4445 (1997).

[38] T. Offermans, S. C. J. Meskers, and R. A. J. Janssen, Chem. Phys. **308**, 125 (2005).

[39] P. Peumans and S. R. Forrest, Chem. Phys. Lett. **398**, 27 (2004).

[40] C. Groves, R. A. Marsh, and N. C. Greenham, J. Chem. Phys. **129**, 114903 (2008).

[41] C. Deibel, T. Strobel, and V. Dyakonov, Phys. Rev. Lett. **103**, 036402 (2009).

[42] M. L. Jones, R. Dyer, N. Clarke, and C. Groves, Phys. Chem. Chem. Phys. **16**, 20310 (2014).

[43] M. L. Jones, B. Chakrabarti, and C. Groves, J. Phys. Chem. C **118**, 85 (2014).

[44] O. Rubel, S. D. Baranovskii, W. Stolz, and F. Gebhard, Phys. Rev. Lett. **100**, 196602 (2008).

[45] S. Tscheuschner, H. Bässler, K. Huber, and A. Köhler, J. Phys. Chem. B **119**, 10359 (2015).

[46] A. P. Arndt, M. Gerhard, A. Quintilla, I. a. Howard, M. Koch, and U. Lemmer, J. Phys. Chem. C **119**, 13516 (2015).

[47] A. P. Arndt, M. Gerhard, M. Koch, U. Lemmer, and I. A. Howard, J. Phys. Chem. C **121**, 6357 (2017).

[48] G. J. Hedley, A. J. Ward, A. Alekseev, C. T. Howells, E. R. Martins, L. a. Serrano, G. Cooke, A. Ruseckas, and I. D. W. Samuel, Nat. Commun. **4**, 2867 (2013).

[49] See Supplemental Material at http://link.aps.org/supplemental/10.1103/PhysRevB.95.195301 for field- and temperature-dependent TRPL data, current-voltage characteristics, PL measurements under forward bias, fluence-dependent quenching measurements, and simulated CT quenching curves with altered parameter sets.

[50] A. Miller and E. Abrahams, Phys. Rev. **120**, 745 (1960).

[51] M. C. Scharber and N. S. Sariciftci, Prog. Polym. Sci. **38**, 1929 (2013).

[52] L. J. A. Koster, S. E. Shaheen, and J. C. Hummelen, Adv. Energy Mater. **2**, 1246 (2012).

[53] V. D. Mihailetchi, J. K. J. Van Duren, P. W. M. Blom, J. C. Hummelen, R. A. J. Janssen, J. M. Kroon, M. T. Rispens, W. J. H. Verhees, and M. M. Wienk, Adv. Funct. Mater. **13**, 43 (2003).

[54] F. Steiner, S. Foster, A. Losquin, J. Labram, and T. D. Anthopoulos, Mater. Horiz. **2**, 113 (2014).

[55] F. Gao, S. Himmelberger, M. Andersson, D. Hanifi, Y. Xia, S. Zhang, J. Wang, J. Hou, A. Salleo, and O. Inganäs, Adv. Mater. **27**, 3868 (2015).

[56] A. A. Bakulin, Y. Xia, H. J. Bakker, O. Inganäs, and F. Gao, J. Phys. Chem. C **120**, 4219 (2016).

[57] Y. Liang, Z. Xu, J. Xia, S.-T. Tsai, Y. Wu, G. Li, C. Ray, and L. Yu, Adv. Mater. **22**, E135 (2010).

[58] C. Poelking and D. Andrienko, J. Am. Chem. Soc. **137**, 6320 (2015).

[59] G. D'Avino, S. Mothy, L. Muccioli, C. Zannoni, L. Wang, J. Cornil, D. Beljonne, and F. Castet, J. Phys. Chem. C **117**, 12981 (2013).

[60] G. D'Avino, L. Muccioli, Y. Olivier, and D. Beljonne, J. Phys. Chem. Lett. **7**, 536 (2016).

[61] M. H. Lee, J. Aragó, and A. Troisi, J. Phys. Chem. C **119**, 14989 (2015).

[62] R. Scholz, R. Luschtinetz, G. Seifert, T. Jägeler-Hoheisel, C. Körner, K. Leo, and M. Rapacioli, J. Phys.: Condens. Matter **25**, 473201 (2013).

[63] M. Wiemer, M. Koch, U. Lemmer, A. B. Pevtsov, and S. D. Baranovskii, Org. Electron. **15**, 2461 (2014).

[64] B. Ebenhoch, S. A. J. Thomson, K. Genevičius, G. Juška, and I. D. Samuel, Org. Electron. **22**, 62 (2015).